J. Fluid Mech. (2014), *vol.* 750, R1, doi:10.1017/jfm.2014.263

JFM RAPIDS
journals.cambridge.org/rapids

Prediction of the hub vortex instability in a wind turbine wake: stability analysis with eddy-viscosity models calibrated on wind tunnel data

F. Viola[1], G. V. Iungo[2], S. Camarri[3,†], F. Porté-Agel[2] and F. Gallaire[1]

[1]Laboratory of Fluid Mechanics and Instabilities, École Polytechnique Fédérale de Lausanne, Lausanne, CH-1015, Switzerland

[2]Wind Engineering and Renewable Energy Laboratory, École Polytechnique Fédérale de Lausanne, Lausanne, CH-1015, Switzerland

[3]Department of Civil and Industrial Engineering, University of Pisa, Pisa 56122, Italy

(Received 28 February 2014; revised 18 April 2014; accepted 6 May 2014;
first published online 30 May 2014)

The instability of the hub vortex observed in wind turbine wakes has recently been studied by Iungo *et al.* (*J. Fluid Mech.*, vol. 737, 2013, pp. 499–526) via local stability analysis of the mean velocity field measured through wind tunnel experiments. This analysis was carried out by neglecting the effect of turbulent fluctuations on the development of the coherent perturbations. In the present paper, we perform a stability analysis taking into account the Reynolds stresses modelled by eddy-viscosity models, which are calibrated on the wind tunnel data. This new formulation for the stability analysis leads to the identification of one clear dominant mode associated with the hub vortex instability, which is the one with the largest overall downstream amplification. Moreover, this analysis also predicts accurately the frequency of the hub vortex instability observed experimentally. The proposed formulation is of general interest for the stability analysis of swirling turbulent flows.

Key words: absolute/convective instability, turbulent flows, vortex instability

1. Introduction

The flow past a wind turbine is characterized by two main large-scale vorticity structures: the helicoidal tip vortices, which detach from the tip of each turbine blade, and the hub vortex, which is a streamwise-oriented vorticity structure located approximately at the wake centre. Several wind tunnel experiments of down-scaled wind turbine models have shown that, besides the frequency connected with the

† Email address for correspondence: s.camarri@ing.unipi.it

shedding of tip vortices, wake velocity signals can present a different spectral contribution with a frequency lower than that of the rotor rotation. In Medici & Alfredsson (2006, 2008), Chamorro & Porté-Agel (2009) and Zhang, Markfort & Porté-Agel (2012), this low-frequency instability was typically ascribed to a global meandering of the wind turbine wake. In large eddy simulations (LES), using actuator disc and actuator line turbine models the far-wake is simulated with sufficient accuracy to reproduce wake meandering (see, for instance, España *et al.* 2011 and Wu & Porté-Agel 2011). More recently, Iungo *et al.* (2013) showed, via local stability analysis performed on time-averaged wind tunnel velocity measurements, that the low frequency clearly detected in the near-wake is related to a single-helix counter-winding instability of the hub vortex, which can also affect the meandering phenomenon in the far-wake. Kang, Yang & Sotiropoulos (2014) confirmed the results of Iungo *et al.* (2013) by carrying out LES simulations, which included all geometrical details of the wind turbine by a curvilinear immersed-boundary method. Recent investigations by Okulov *et al.* (2014) show experimentally, through laser doppler anemometry (LDA) and particle image velocimetry (PIV) visualization, the rotation of the helical vortex core.

The main limitation of the analysis presented by Iungo *et al.* (2013), which is focused on the hub vortex instability, is that the instability observed experimentally was not predicted through the local stability analysis as the unstable mode with the largest growth rate. Indeed, it was necessary to use the instability frequency of the hub vortex, which was determined via wind tunnel measurements, as an additional input for the stability analysis in order to detect the mode associated with the hub vortex instability. The main reason for difficulties in the identification of the dominant unstable mode by the sole stability analysis was attributed to the neglect of the Reynolds stresses in the Orr–Sommerfeld equations.

In this paper, a stability analysis is performed by taking into account the effects of the Reynolds stresses by means of eddy-viscosity models, which are calibrated on the wind tunnel data. Other studies in the literature have considered eddy-viscosity models to close the linearized equations for the coherent velocity field in a turbulent flow (see, e.g. Reynolds & Hussain 1972; Bottaro, Soueid & Galletti 2006; Crouch, Garbaruk & Magidov 2007; Cossu, Pujals & Depardon 2009; Meliga, Pujals & Serre 2012). A similar but more sophisticated closure is proposed by Kitsios *et al.* (2010, 2011). For the present investigation three eddy-viscosity models are considered. One model is based on the assumption of a uniform eddy viscosity for each streamwise location, whereas for the other two models a mixing length is estimated. In this paper it is shown that with the proposed improved formulation, stability analysis allows not only the unambiguous identification of the hub vortex instability, but also the accurate prediction of its instability frequency.

The paper is organized as follows: the formulation of the stability analysis is presented in § 2 by taking the Reynolds stresses into account. The wind tunnel data are then described in § 3, while the three eddy-viscosity models and their calibration against the wind tunnel data are reported in § 4. The characterization of the hub vortex instability is presented in § 5. Finally, conclusions are drawn in § 6.

2. Problem formulation

2.1. *Triple decomposition and linearized equations for the coherent perturbation*

Following the approach proposed in Reynolds & Hussain (1972), the unsteady flow, $\boldsymbol{U}(\boldsymbol{x}, t)$, is decomposed into the time-averaged base flow, $\overline{\boldsymbol{U}}(\boldsymbol{x})$, the coherent

fluctuation, $\tilde{\boldsymbol{u}}(\boldsymbol{x}, t)$, and the turbulent motion, $\boldsymbol{u}'(\boldsymbol{x}, t)$,

$$\boldsymbol{U} = \overline{\boldsymbol{U}} + \tilde{\boldsymbol{u}} + \boldsymbol{u}', \tag{2.1}$$

where the sum of the time-averaged flow and the coherent fluctuation coincides with the ensemble-averaged flow $\langle \boldsymbol{U} \rangle = \overline{\boldsymbol{U}} + \tilde{\boldsymbol{u}}$ (see also Reau & Tumin 2002).

The stability of the flow is given by the tendency of $\tilde{\boldsymbol{u}}$ to grow (unstable) or decay (stable) in time and space. Thus, stability can be verified by a modal analysis of the linearized dynamics of $\tilde{\boldsymbol{u}}$. To this purpose the nonlinear evolution of the coherent perturbation for an incompressible flow can be written as (see, e.g. Reynolds & Hussain 1972)

$$\nabla \cdot \tilde{\boldsymbol{u}} = 0, \tag{2.2}$$

$$\frac{\partial \tilde{\boldsymbol{u}}}{\partial t} + \nabla \tilde{\boldsymbol{u}} \cdot \overline{\boldsymbol{U}} + \nabla \overline{\boldsymbol{U}} \cdot \tilde{\boldsymbol{u}} = -\nabla \tilde{p} + \frac{1}{Re} \Delta \tilde{\boldsymbol{u}} - \nabla \cdot [\tilde{\boldsymbol{u}}\tilde{\boldsymbol{u}} - \overline{\tilde{\boldsymbol{u}}\tilde{\boldsymbol{u}}}] - \nabla \cdot [\langle \boldsymbol{u}'\boldsymbol{u}' \rangle - \overline{\boldsymbol{u}'\boldsymbol{u}'}], \tag{2.3}$$

where variables t and p represent time and pressure, respectively. In the framework of a linear analysis with respect to the coherent fluctuations $\tilde{\boldsymbol{u}}$, the third term of the right-hand side is neglected. However, the system of equations is not closed and the last term of the right-hand side, related to the turbulent diffusion, has to be modelled. As in Reynolds & Hussain (1972) and Cossu *et al.* (2009), the linear relationship between the strain rate and the Reynolds stresses is considered here. In the following two equations, the Boussinesq hypothesis is written using time and ensemble averaging, respectively,

$$\begin{cases} -\overline{\boldsymbol{u}'\boldsymbol{u}'} + \frac{2}{3}\overline{q}\boldsymbol{I} \simeq \nu_t^m [\nabla + \nabla^T] \overline{\boldsymbol{U}}, \\ -\langle \boldsymbol{u}'\boldsymbol{u}' \rangle + \frac{2}{3}\langle q \rangle \boldsymbol{I} \simeq \nu_t^e [\nabla + \nabla^T] \langle \boldsymbol{U} \rangle, \end{cases} \tag{2.4}$$

where q is the turbulent kinetic energy (TKE) and $\boldsymbol{I}$ is the 3×3 identity matrix. The eddy viscosity depends on $\overline{\boldsymbol{U}}$ (i.e. $\nu_t^m(\overline{\boldsymbol{U}})$) in the case of time averaging and on $\langle \boldsymbol{U} \rangle$ (i.e. $\nu_t^e(\langle \boldsymbol{U} \rangle) = \nu_t^e(\overline{\boldsymbol{U}} + \tilde{\boldsymbol{u}})$) in the case of ensemble averaging. By linearizing ν_t^e at first order with respect to $\tilde{\boldsymbol{u}}$, it is possible to rewrite it as the sum of one function of the mean flow and one linear function of the coherent fluctuation, $\nu_t^e(\overline{\boldsymbol{U}} + \tilde{\boldsymbol{u}}) \simeq \nu_t^e(\overline{\boldsymbol{U}}) + \nabla_{\boldsymbol{U}} \nu_t^e(\overline{\boldsymbol{U}}) \cdot \tilde{\boldsymbol{u}}$ (see appendix A). In order to determine the relation between $\nu_t^m(\overline{\boldsymbol{U}})$ and $\nu_t^e(\overline{\boldsymbol{U}})$, the second equation in (2.4) is averaged in time. Since the time average of an ensemble average corresponds to the time average itself ($\overline{\langle \cdot \rangle} = \overline{\cdot}$), we obtain the following set of identities:

$$\begin{aligned} -\overline{\boldsymbol{u}'\boldsymbol{u}'} + \tfrac{2}{3}\overline{q}\boldsymbol{I} &= \overline{-\langle \boldsymbol{u}'\boldsymbol{u}' \rangle + \tfrac{2}{3}\langle q \rangle \boldsymbol{I}} \simeq \overline{\nu_t^e(\langle \boldsymbol{U} \rangle)[\nabla + \nabla^T]\langle \boldsymbol{U} \rangle} \\ &\simeq \overline{\nu_t^e(\overline{\boldsymbol{U}})[\nabla + \nabla^T]\overline{\boldsymbol{U}}} + \overline{(\nabla_{\boldsymbol{U}} \nu_t^e(\overline{\boldsymbol{U}}) \cdot \tilde{\boldsymbol{u}})[\nabla + \nabla^T]\overline{\boldsymbol{U}}} + \overline{\nu_t^e(\overline{\boldsymbol{U}})[\nabla + \nabla^T]\tilde{\boldsymbol{u}}} \\ &\quad + \overline{(\nabla_{\boldsymbol{U}} \nu_t^e(\overline{\boldsymbol{U}}) \cdot \tilde{\boldsymbol{u}})[\nabla + \nabla^T]\tilde{\boldsymbol{u}}} \simeq \nu_t^e(\overline{\boldsymbol{U}})[\nabla + \nabla^T]\overline{\boldsymbol{U}}, \end{aligned} \tag{2.5}$$

where the second and third terms of the right-hand side in the last identity are rigorously null because the averaged quantities depend linearly on $\tilde{\boldsymbol{u}}$. The fourth term is neglected since it is of higher order in $\tilde{\boldsymbol{u}}$. Consequently, the last (quasi-)identity follows and, together with the first equation in (2.4), it leads to the result $\nu_t^e(\overline{\boldsymbol{U}}) = \nu_t^m(\overline{\boldsymbol{U}})$.

According to the previous results, the term $\langle \boldsymbol{u}'\boldsymbol{u}' \rangle - \overline{\boldsymbol{u}'\boldsymbol{u}'}$ can be modelled as

$$\begin{aligned}\langle \boldsymbol{u}'\boldsymbol{u}' \rangle - \overline{\boldsymbol{u}'\boldsymbol{u}'} \simeq & -\nu_t^e(\overline{\boldsymbol{U}}+\tilde{\boldsymbol{u}})[\boldsymbol{\nabla}+\boldsymbol{\nabla}^T]\langle \boldsymbol{U} \rangle + \nu_t^m(\overline{\boldsymbol{U}})[\boldsymbol{\nabla}+\boldsymbol{\nabla}^T]\overline{\boldsymbol{U}} + \tfrac{2}{3}\langle q \rangle \boldsymbol{I} - \tfrac{2}{3}\overline{q}\boldsymbol{I} \\ \simeq & -\nu_t^e(\overline{\boldsymbol{U}})[\boldsymbol{\nabla}+\boldsymbol{\nabla}^T]\overline{\boldsymbol{U}} - (\boldsymbol{\nabla}_{\boldsymbol{U}}\nu_t^e(\overline{\boldsymbol{U}})\cdot\tilde{\boldsymbol{u}})[\boldsymbol{\nabla}+\boldsymbol{\nabla}^T]\overline{\boldsymbol{U}} - \nu_t^e(\overline{\boldsymbol{U}})[\boldsymbol{\nabla}+\boldsymbol{\nabla}^T]\tilde{\boldsymbol{u}} \\ & - (\boldsymbol{\nabla}_{\boldsymbol{U}}\nu_t^e(\overline{\boldsymbol{U}})\cdot\tilde{\boldsymbol{u}})[\boldsymbol{\nabla}+\boldsymbol{\nabla}^T]\tilde{\boldsymbol{u}} + \nu_t^m(\overline{\boldsymbol{U}})[\boldsymbol{\nabla}+\boldsymbol{\nabla}^T]\overline{\boldsymbol{U}} + \tfrac{2}{3}\langle q \rangle \boldsymbol{I} - \tfrac{2}{3}\overline{q}\boldsymbol{I}.\end{aligned} \tag{2.6}$$

The first and fifth terms in the last identity cancel out since $\nu_t^e(\overline{\boldsymbol{U}}) = \nu_t^m(\overline{\boldsymbol{U}})$. The fourth term is neglected because it is of higher order in $\tilde{\boldsymbol{u}}$, yielding

$$\langle \boldsymbol{u}'\boldsymbol{u}' \rangle - \overline{\boldsymbol{u}'\boldsymbol{u}'} \simeq -(\boldsymbol{\nabla}_{\boldsymbol{U}}\nu_t^e(\overline{\boldsymbol{U}})\cdot\tilde{\boldsymbol{u}})[\boldsymbol{\nabla}+\boldsymbol{\nabla}^T]\overline{\boldsymbol{U}} - \nu_t^e(\overline{\boldsymbol{U}})[\boldsymbol{\nabla}+\boldsymbol{\nabla}^T]\tilde{\boldsymbol{u}} + \tfrac{2}{3}\langle q \rangle \boldsymbol{I} - \tfrac{2}{3}\overline{q}\boldsymbol{I}. \tag{2.7}$$

As in Reynolds & Hussain (1972) and Kitsios *et al.* (2010), we assume that the phase-averaging process affects the turbulence structure but not the energy, i.e. $\langle q \rangle \simeq \overline{q}$, obtaining

$$\langle \boldsymbol{u}'\boldsymbol{u}' \rangle - \overline{\boldsymbol{u}'\boldsymbol{u}'} \simeq -(\boldsymbol{\nabla}_{\boldsymbol{U}}\nu_t^e(\overline{\boldsymbol{U}})\cdot\tilde{\boldsymbol{u}})[\boldsymbol{\nabla}+\boldsymbol{\nabla}^T]\overline{\boldsymbol{U}} - \nu_t^e(\overline{\boldsymbol{U}})[\boldsymbol{\nabla}+\boldsymbol{\nabla}^T]\tilde{\boldsymbol{u}}. \tag{2.8}$$

The term $\nu_t^e(\overline{\boldsymbol{U}}) = \nu_t^m(\overline{\boldsymbol{U}})$ in (2.8) can be evaluated from the statistics of the experimental data, as in Kitsios *et al.* (2010), while the term $\boldsymbol{\nabla}_{\boldsymbol{U}}\nu_t(\overline{\boldsymbol{U}})\cdot\tilde{\boldsymbol{u}}$ is obtained by the linearization of the turbulence model used to close the equations, as detailed in appendix A. When (2.8) is substituted into (2.2), the linear evolution of the coherent perturbation $\tilde{\boldsymbol{u}}$ with modelled Reynolds stresses is retrieved:

$$\begin{aligned}\frac{\partial \tilde{\boldsymbol{u}}}{\partial t} + \boldsymbol{\nabla}\tilde{\boldsymbol{u}}\cdot\overline{\boldsymbol{U}} + \boldsymbol{\nabla}\overline{\boldsymbol{U}}\cdot\tilde{\boldsymbol{u}} = & -\boldsymbol{\nabla}\tilde{p} + \frac{1}{Re}\Delta\tilde{\boldsymbol{u}} + \boldsymbol{\nabla}\cdot(\nu_t(\overline{\boldsymbol{U}})[\boldsymbol{\nabla}+\boldsymbol{\nabla}^T]\tilde{\boldsymbol{u}}) \\ & + \boldsymbol{\nabla}\cdot((\boldsymbol{\nabla}_{\boldsymbol{U}}\nu_t(\overline{\boldsymbol{U}})\cdot\tilde{\boldsymbol{u}})[\boldsymbol{\nabla}+\boldsymbol{\nabla}^T]\overline{\boldsymbol{U}}).\end{aligned} \tag{2.9}$$

Equation (2.9) is analogous to the one used in Reynolds & Hussain (1972), del Àlamo & Jimenez (2006) and Cossu *et al.* (2009), but the last term on the right-hand side is included to take the linearization of the turbulence model into account. This corresponds to a generalization of the formulation of Crouch *et al.* (2007) and Meliga *et al.* (2012) based on the Spalart–Allmaras model. From now on the subscripts for the eddy viscosity, e and m, will not be specified any longer because they are redundant.

2.2. *Application to parallel flow*

In the framework of weakly non-parallel stability analysis, (2.9) is now applied to a parallel flow $\overline{\boldsymbol{U}} = (\overline{U}_x, \overline{U}_\theta, 0)$ extracted at a given streamwise location, since experiments have shown a negligible radial velocity component (Iungo *et al.* 2013). This allows for a modal expansion of the coherent fluctuation in the following form:

$$\tilde{\boldsymbol{u}}(x, \theta, r, t) = \hat{\boldsymbol{u}}(r)\exp(\mathrm{i}kx + \mathrm{i}m\theta - \mathrm{i}\omega t), \tag{2.10}$$

where k and m are the axial and azimuthal wavenumbers respectively, and ω is the frequency. When this modal form is substituted into (2.9), an eigenvalue problem is obtained. In the temporal stability analysis k is real and assigned, while ω is the complex eigenvalue of the problem. The opposite choice is made for the spatial stability analysis. In both cases, m is a free integer parameter.

For the stability analysis, equation (2.9) and the continuity equation are discretized using a code based on a Chebyshev spectral collocation method. In the present analysis the number of collocation points is $N = 120$ and the size of the domain

in the radial direction is $r_{max}/d = 50$. This choice provides the convergence of the most unstable eigenvalue with a five-digit accuracy, which is sufficient for the present purposes.

3. Wind tunnel measurements

Velocity measurements of the wake produced by a down-scaled three-bladed wind turbine were performed in the boundary-layer wind tunnel of the Wind Engineering and Renewable Energy Laboratory (WIRE) of the École Polytechnique Fédérale de Lausanne (EPFL). For details on the experimental set-up and measurement techniques we refer to Iungo *et al.* (2013). The tip speed ratio of the turbine (TSR), which is the ratio between the speed of the blade tip and the oncoming velocity at hub height ($U_{hub} = 6.9$ m s^{-1}), is equal to 4.6 with a free stream turbulence level equal to 6 %. The stability equations and the subsequent results are normalized using U_{hub} as the reference velocity and the rotor diameter, $d = 0.152$ m, as the reference length, leading to a flow Reynolds number equal to 72 000. For these tests the mean rotational frequency was $f_{hub} \approx 66$ Hz and the frequency connected with the tip vortex shedding was equal to three times f_{hub}, i.e. $f_{tip\,vortices} \approx 198$ Hz. The frequency related to the hub vortex instability was 21 Hz, i.e. approximately equal to 0.32 f_{hub}. This instability frequency corresponds to a non-dimensional pulsation of $\omega_{hub\,vortex} = 2\pi d f_{hub\,vortex}/U_{hub} = 2.9$.

Since the turbine is placed outside the boundary layer and immersed in a uniform oncoming flow, the mean wake flow produced is axisymmetric. Experiments show also a negligible radial component of the velocity, which is thus completely characterized by the axial, $\overline{U}_x$, and azimuthal, $\overline{U}_\theta$, velocity components. The experimental time-averaged velocity field and the Reynolds stresses used for the stability analysis are plotted in figure 1. Velocity measurements cannot be performed at a downstream distance smaller than 0.5 d with hot-wire anemometers and multi-hole (Cobra) probes. Indeed, at those locations the strong axial velocity deficit and the large tangential velocity produce an angle between the probe axis and the velocity vector larger than 45°, which is the limit angle to perform velocity measurements with an acceptable accuracy. Apart from this technical limitation, in the very near-wake the rollup of the wake vorticity structures produces strong velocity gradients along the streamwise direction, thus the weakly non-parallel assumption adopted for the stability analysis cannot be ensured. In figure 1 the reported vertical lines correspond to the sections where local stability analysis was carried out, i.e. $x/d = 0.5, 0.75, 1, 1.25, 1.5, 2$. On the other hand, sections at $x/d > 2$ are not considered here since in that region the growth rates are significantly smaller in comparison with the ones evaluated for the upstream locations (see Iungo *et al.* 2013).

4. Eddy-viscosity models

4.1. *Description of the considered turbulence closure models*

As already pointed out, the Boussinesq hypothesis yields

$$\overline{R} = \overline{\boldsymbol{u}'\boldsymbol{u}'} \simeq -2\nu_t \overline{S} + \tfrac{2}{3}\overline{q}\boldsymbol{I}, \tag{4.1}$$

where $\boldsymbol{R}$ is the Reynolds stress tensor and $\boldsymbol{S}$ is the strain rate tensor. In the framework of a local stability analysis of a wind turbine wake flow, we have $\overline{U}_r = 0$ and $\partial\overline{\boldsymbol{U}}/\partial\theta = \partial\overline{\boldsymbol{U}}/\partial x = 0$, which implies that the term $\overline{R}_{x\theta} = \overline{u'_\theta u'_x}$ is null, and the model leads to null

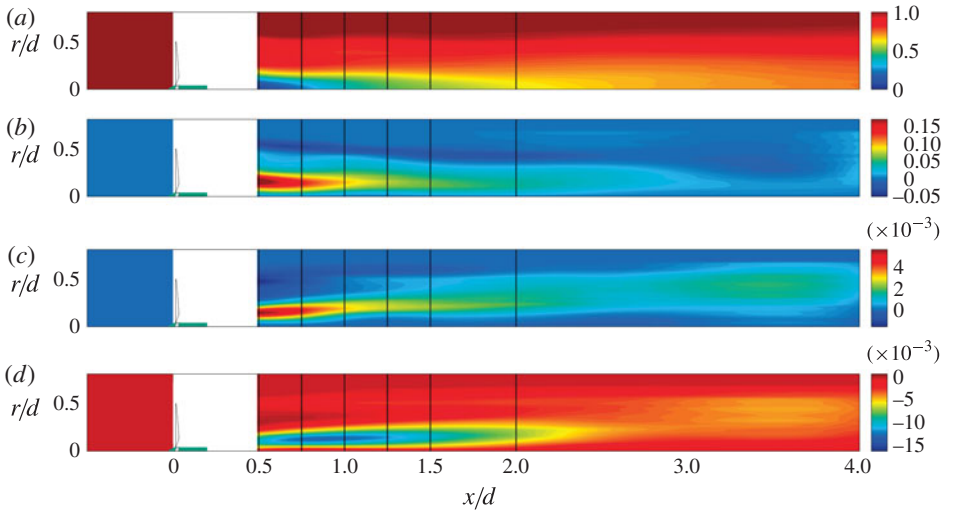

FIGURE 1. Non-dimensional mean velocity components and tangential Reynolds stresses acquired in the wind tunnel. (*a*) Axial $\overline{U}_x/U_{hub}$ and (*b*) azimuthal $\overline{U}_\theta/U_{hub}$ velocities, (*c*) $\overline{u'_r u'_\theta}/U^2_{hub}$ and (*d*) $\overline{u'_r u'_x}/U^2_{hub}$. Vertical lines depict the streamwise positions where local stability analysis has been carried out. In the white region measurements are not available.

normal stresses (see Kitsios *et al.* 2010). Consequently, the only non-null components of the modelled tensor $\overline{R}$ are $\overline{R}_{r\theta}$, $\overline{R}_{rx}$ and their symmetric counterparts.

Three different turbulence models are considered here, which are concisely described in the following. The first is a uniform eddy-viscosity model, in which the eddy viscosity, ν_t, in (4.1) is assumed to be only a function of the streamwise location, and it is the only unknown closure parameter of the resulting model. The same model for a local stability analysis is employed, for instance, in Oberleithner, Paschereit & Wygnanski (2014). The other two turbulence models are based on the concept of a mixing length, l_m, in order to define the eddy viscosity. The mixing length, l_m, is a function of the streamwise position and it is the only unknown parameter of the turbulence closure model. The second considered model is the classical mixing-length model, in which ν_t is related to l_m as follows:

$$\nu_t(r) = l_m^2 \left| \frac{\partial \overline{U}_x}{\partial r} \right|. \tag{4.2}$$

The third model is a generalized mixing-length model for swirling flows (see appendix A and Pope 2000 for more details):

$$\nu_t(r) = l_m^2 (2\overline{S} : \overline{S})^{1/2} = l_m^2 \left[\left(r \frac{\partial}{\partial r} \left(\frac{\overline{U}_\theta}{r} \right) \right)^2 + \left(\frac{\partial \overline{U}_x}{\partial r} \right)^2 \right]^{1/2}. \tag{4.3}$$

4.2. *Calibration of the turbulence closure models against wind tunnel data*

The free parameters of the eddy-viscosity models are calibrated by using the statistics of the experimental velocity data at each streamwise section. Specifically, a best-fit strategy between the measured Reynolds stresses and the modelled ones, minimizing

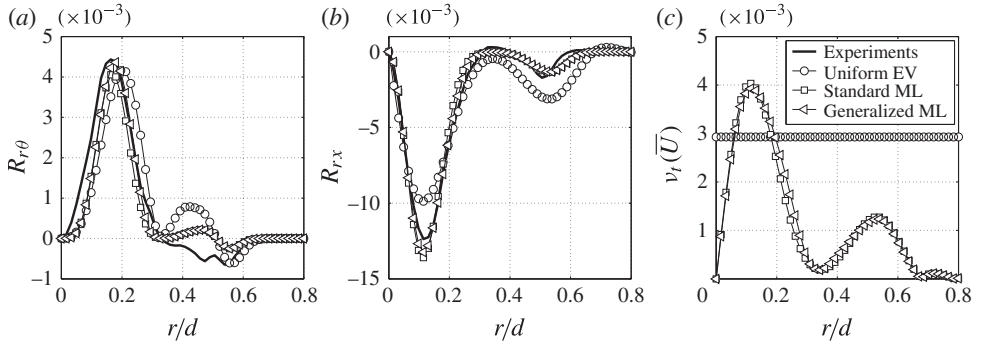

FIGURE 2. Calibration of the closure turbulence models against the wind tunnel data (solid curve) for the downstream position $x/d = 0.75$. The Reynolds stresses (*a*) $\overline{R}_{r\theta}$ and (*b*) $\overline{R}_{rx}$ are shown. The symbols refer to the three calibrated models, detailed in the legend (EV and ML stand for eddy viscosity and mixing length, respectively). The resulting eddy viscosities obtained for the different models are then reported in (*c*). The *uniform* EV appears as a straight line.

the norm of the residuals of (4.1), has been adopted. For the uniform eddy-viscosity model, the value of ν_t, which is independent of r, is estimated at each streamwise location by minimizing the functional,

$$\nu_t(x): \ \min_{\nu_t} \sum_j \left\| (\overline{R}(r_j, x) - 2/3\overline{q}(r_j, x)\boldsymbol{I}) - \left(-2\nu_t(x)\overline{S}(r_j, x)\right) \right\|^2, \tag{4.4}$$

where the r_j are the discrete radial positions where experimental data are acquired.

In the case of mixing-length turbulence models, at a given x-location the function to minimize is obtained by substituting in (4.4) the mixing-length model expressions for ν_t ((4.2) and (4.3)) and optimizing with respect to the scalar l_m, which varies with x and is independent of r. It should be noted that direct use of the statistics of the experimental velocity field needs a further assumption, since measurements include the saturated coherent fluctuation $\widetilde{\overline{u}_i}\widetilde{\overline{u}_j}$, which cannot be modelled using the Boussinesq approximation. Thus, the best-fit strategy used requires that the stresses $\widetilde{\overline{u}_i}\widetilde{\overline{u}_j}$ are small in comparison with $\overline{u_i'u_j'}$ (see, for instance, Kitsios *et al.* 2010). This assumption is very reasonable for high-Reynolds-number turbulent flows, as for the considered case, and it is supported *a posteriori* by the accuracy of the obtained stability results (see § 5).

An example of the calibration fitting procedure performed for all the considered models is shown in figure 2 for the measurements acquired at $x/d = 0.75$. In figure 2(*a–b*) the Reynolds stresses modelled from the experimental strain rate tensor through the calibrated turbulence closure models are compared with the ones directly measured through the wind tunnel tests. It is evident that a fair accuracy is generally achieved through the fitting procedure. Specifically, the Reynolds stress peaks connected with the presence of the hub vortex, observed at $r/d \simeq 0.15$ for both $R_{r\theta}$ and R_{rx}, are well reproduced by the models. However, some differences can be observed in proximity to the tip vortex location at $r/d \simeq 0.5$, especially with respect to $R_{r\theta}$. This feature suggests that the turbulence closure models and the calibration fitting procedure could be improved. However, in § 5 we will show that the results of the stability analysis are very robust with respect to the differences in the calibrated ν_t, which arise from the use of different closure models and/or due to the accuracy of the calibration procedure.

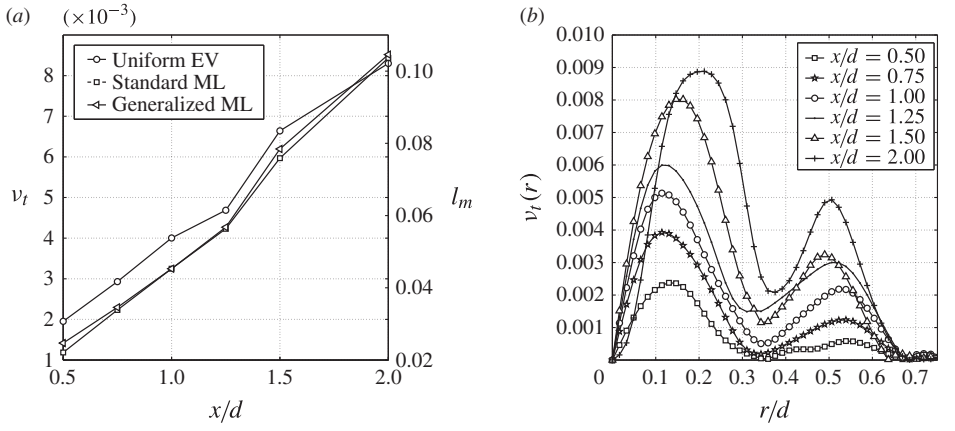

FIGURE 3. Calibration of the closure turbulence models. (*a*) Superposition of ν_t in the case of uniform EV (left ordinate axis) and l_m for standard and generalized ML (right ordinate axis), as a function of the streamwise position x/d. (*b*) Radial profiles of ν_t evaluated via the generalized mixing-length model for different streamwise locations.

Figure 2(*c*) represents the tuned eddy viscosity resulting from the models. It should be noted that ν_t is constant for the uniform eddy-viscosity (EV) model and its normalized value of the eddy viscosity evaluated at $x/d = 0.75$ is $\nu_t \simeq 0.0029$. In this case the stability analysis of the turbulent mean flow reduces to a laminar calculation carried out using a locally modified Reynolds number Re^*, defined as $(1/Re^*) = (1/Re) + \nu_t$. In the case of mixing-length (ML) models, ν_t is a function of the radial position r/d and its value in the hub vortex region is comparable with the one obtained with the uniform eddy-viscosity model.

The described best-fit procedure has been carried out for all the considered streamwise sections, leading to results analogous to the ones presented for the location $x/d = 0.75$. In order to provide further information on the trend of the free model parameters as a function of the streamwise location, x/d, we report in figure 3(*a*) the calibrated values of ν_t and l_m. This figure shows that ν_t and l_m obtained through the calibration procedure grow almost linearly with x/d, implying that the diffusive effects due to turbulence increase on moving downstream. This result is in qualitative agreement with the experiments where it was observed that the hub vortex is almost completely diffused for $x/d > 3$ (Iungo *et al.* 2013). Moreover, for the two mixing-length models, the obtained values for l_m almost coincide since the expression $2\overline{S} : \overline{S}$ is dominated by the term $\partial \overline{U}_x/\partial r$ in the considered flow (compare (4.2) with (4.3)). Lastly, figure 3(*b*) shows that the profiles of ν_t obtained by the generalized mixing-length model as a function of the radial position remain similar at the different streamwise sections. In particular, they are characterized by a higher peak located in the proximity of the hub vortex position, and a smaller one in proximity to the tip vortex location. The same conclusions apply for the standard mixing-length model. The eddy-viscosity profiles in figure 3(*b*) are then introduced into the local linear stability analysis through the term $\nu_t(\overline{\boldsymbol{U}})$ of (2.9).

5. Stability analysis results

5.1. *Temporal stability analysis and mode selection*

Figure 4 depicts the results of temporal stability analysis carried out at the streamwise location $x/d = 0.5$, (*a*) neglecting the contribution of the Reynolds stresses, (*b*) using

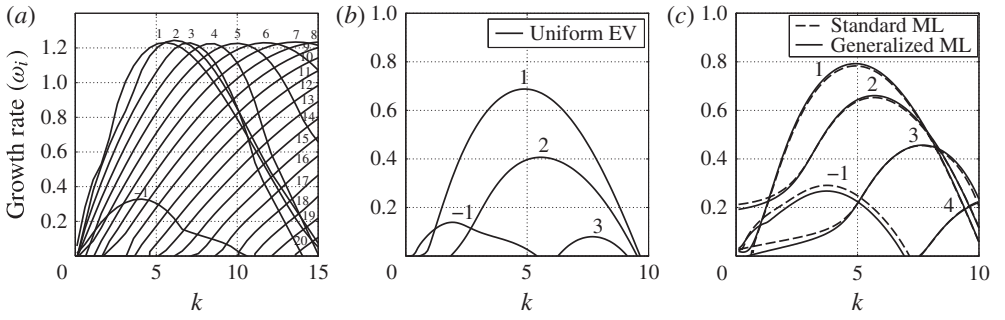

FIGURE 4. Temporal analysis results at section $x/d = 0.5$ (*a*) without Reynolds stresses, (*b*) with the uniform eddy-viscosity model and (*c*) with the generalized and standard (dashed line) mixing-length models. Growth rates are reported as a function of the axial wavenumber k, and each branch corresponds to a different azimuthal wavenumber m.

the uniform eddy-viscosity model and (*c*) using both the standard and the generalized mixing-length models. For each case the growth rate, ω_i, is reported as a function of the axial wavenumber, k, while each branch corresponds to a different azimuthal wavenumber, m. As in Iungo *et al.* (2013), when Reynolds stresses are neglected, the temporal stability analysis predicts many unstable modes, and it is not possible to identify a single dominant mode as observed in the experiments. Conversely, figures 4(*b*,*c*) show that, when a model for the turbulent diffusion is introduced, the temporal stability analysis identifies a clearly dominant unstable mode among only four unstable modes detected. Specifically, the higher-wavenumber modes are more damped since the diffusion term is proportional to k^2 and m^2, and the mode with $m = 1$ results to be the one with the largest growth rate at every considered downstream position. This mode, not shown here for the sake of brevity, is the single-helix counter-winding mode characterized experimentally by Iungo *et al.* (2013). Thus, the present results demonstrate the important role of the turbulent diffusion mechanism in the evolution of the perturbation, and that even a simple eddy-viscosity model is sufficient to improve the results of the local temporal stability analysis, so as to identify a clearly dominant unstable mode. Moreover, figures 4(*b*,*c*) show that the differences among the results obtained by the different closure turbulence models are moderate with respect to the detection of a dominant unstable mode, and that mixing-length models damp the modes associated with higher frequencies slightly less. Similar results have been found for all the analysed streamwise locations.

5.2. *Spatial stability analysis, integral growth rate and instability frequency prediction*

In the framework of local stability analysis of weakly non-parallel flows, the integral amplification factor of each unstable mode is determined by integrating in the streamwise direction its spatial growth rate, $-k_i(m, \omega, x)$, which is obtained from dedicated spatial stability analyses. Thus, $-k_i(m, \omega, x)$ is integrated from a given streamwise position, x_0, up to the downstream position where the mode becomes stable again, x_s,

$$G(m, \omega) = \exp \int_{x_0}^{x_S} -k_i(m, \omega, x')\mathrm{d}x'. \tag{5.1}$$

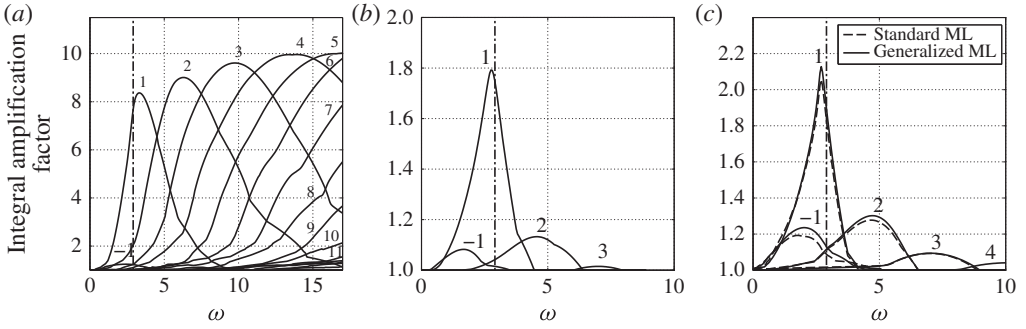

FIGURE 5. Integral amplification factor in the wake (*a*) without Reynolds stresses, (*b*) with the uniform eddy-viscosity model and (*c*) with the generalized and the standard (dashed line) mixing-length models. Growth rates are reported as a function of the frequency ω, and each branch corresponds to a different azimuthal wavenumber m. The vertical dash-dotted line represents the frequency of the hub vortex instability measured experimentally, corresponding to a non-dimensional pulsation $\omega_{hub\ vortex} = 2.9$.

Here, $G(\omega, m)$ represents the overall amplification of the mode m at the frequency ω within the wake, after it has undergone its entire amplification process. We recall that $G(m, \omega)$ is a synthesis of the results obtained by local spatial stability analyses carried out at different streamwise sections.

In figure 5 the integral amplification factors of the unstable modes are reported as a function of the frequency ω. As shown in figure 5(*a*), when the Reynolds stresses are neglected many unstable modes exist and, as for the temporal analysis, it is not possible to select a dominant mode without considering as additional input the instability frequency detected experimentally. On the other hand, the use of an eddy-viscosity model allows a clear mode identification, as shown in figure 5(*b*,*c*), and the mode associated with $m = 1$ is the most spatially amplified one. Its amplification factor has a clear and definitely dominant peak at a frequency ω_f, which is almost coincident with the one measured experimentally ($\omega_{hub\ vortex} = 2.9$ is reported in figure 5 as a vertical dash-dotted line). For a more quantitative comparison, the relative error between the experimental instability frequency ($\omega_{hub\ vortex}$) and the predicted frequency ω_f has been computed: a relative error of approximately 7.1 % is obtained for the mixing-length models, and this error is further decreased to 5.3 % when the uniform eddy-viscosity model is used.

6. Conclusions

In this paper eddy-viscosity models are applied in order to take into account turbulence in the stability analysis of the time-averaged flow field past a wind turbine. The work is motivated by a previous investigation, Iungo *et al.* (2013), in which stability analysis was carried out by neglecting the Reynolds stresses. In that study, the characterization of the hub vortex instability was achieved by using as additional input to the stability analysis the instability frequency, which was evaluated via wind tunnel experiments. Here, three turbulence closure models have been considered: a uniform eddy-viscosity model and two mixing-length models (a standard one and a generalized one for swirling flows). The free parameters of the models have been tuned using the available wind tunnel data. Using the considered models, the number of unstable modes detected via stability analysis is drastically reduced, and

the spatially integrated growth factors clearly indicate one dominant unstable mode, i.e. the single-helix counter-winding mode observed experimentally by Iungo *et al.* (2013). Its instability frequency is also predicted with a very good agreement with the experimental evidence.

The present results show that the use of calibrated turbulence models in the stability analysis of the time-averaged flow field allows not only the characterization of the hub vortex instability, but also the accurate prediction of the associated instability frequency. This result is obtained using simple algebraic closures, properly calibrated, even if the framework proposed here can include more complex Reynolds averaged Navier–Stokes models as well. The fact that the mode identification is the result of the sole stability analysis, and that it does not require any additional external information, is of crucial importance for many further applications of the proposed method. Specifically, this technique should allow for significant improvements in the prediction of the downstream recovery of wind turbine wakes, and ultimately their control. For this reason, and also due to the accuracy observed in the present application, we believe that this strategy and the results discussed in this paper are also of general interest for the stability analysis of turbulent swirling flows.

Acknowledgements

The authors wish to acknowledge V. Mantic-Lugo and Professor C. Meneveau for stimulating discussions.

Appendix A

In order to include the effect of turbulent fluctuations in the equation of the coherent perturbation (2.9), the gradient of the eddy viscosity with respect to the velocity evaluated in the mean flow configuration, $\overline{\boldsymbol{U}}$, needs to be calculated. While it is undetermined and set to zero in the uniform eddy-viscosity model, it is now evaluated for the two mixing-length models studied in this paper. In the case of standard mixing length

$$\nu_t^e(\langle \boldsymbol{U} \rangle) = l_m^2 \left| \frac{\partial \langle U_x \rangle}{\partial r} \right| \simeq l_m^2 \left| \frac{\partial \overline{U}_x}{\partial r} \right| + \operatorname{sign}\left(\frac{\partial \overline{U}_x}{\partial r} \right) l_m^2 \frac{\partial \tilde{u}_x}{\partial r} = \nu_t^e(\overline{\boldsymbol{U}}) + \boldsymbol{\nabla}_{\boldsymbol{U}} \nu_t^e(\overline{\boldsymbol{U}}) \cdot \tilde{\boldsymbol{u}}. \quad (A\,1)$$

Now, considering the generalized expression for the mixing-length model (see Pope 2000), in the case of an axisymmetric locally parallel mean flow

$$\nu_t^e(\langle \boldsymbol{U} \rangle) = l_m^2 (2\langle S \rangle : \langle S \rangle)^{1/2} = l_m^2 \left[\left(r \frac{\partial \langle U_\theta \rangle / r}{\partial r} \right)^2 + \left(\frac{\partial \langle U_x \rangle}{\partial r} \right)^2 \right]^{1/2}. \quad (A\,2)$$

By splitting, as usual, the ensemble-averaged flow into the time-averaged flow plus the coherent fluctuation, and recalling that $\sqrt{1+x} = 1 + (1/2)x + O(x^2)$ for $x \to 0$,

$$\begin{aligned} \nu_t^e(\langle \boldsymbol{U} \rangle) \;=\; & l_m^2 (2\langle S \rangle : \langle S \rangle)^{1/2} \simeq l_m^2 (2\overline{S} : \overline{S})^{1/2} + \frac{l_m^2}{(2\overline{S} : \overline{S})^{1/2}} \\ & \times \left[r \frac{\partial \overline{U}_\theta / r}{\partial r} \left(\frac{\partial \tilde{u}_\theta}{\partial r} + \frac{\tilde{u}_\theta}{r} \right) + \frac{\partial \overline{U}_x}{\partial r} \frac{\partial \tilde{u}_x}{\partial r} \right] = \nu_t^e(\overline{\boldsymbol{U}}) + \boldsymbol{\nabla}_{\boldsymbol{U}} \nu_t^e(\overline{\boldsymbol{U}}) \cdot \tilde{\boldsymbol{u}}. \quad (A\,3) \end{aligned}$$

It should be noted that if $\overline{U}_\theta = 0$, $\nu_t^e(\overline{\boldsymbol{U}})$ and $\boldsymbol{\nabla}_{\boldsymbol{U}} \nu_t^e(\overline{\boldsymbol{U}}) \cdot \tilde{\boldsymbol{u}}$ reduce to the ones of standard mixing length.

References

DEL ÀLAMO, J. C. & JIMENEZ, J. 2006 Linear energy amplification in turbulent channels. *J. Fluid Mech.* **559**, 205–213.

BOTTARO, A., SOUEID, H. & GALLETTI, B. 2006 Formation of secondary vortices in turbulent square-duct flow. *AIAA J.* **44** (4), 803–811.

CHAMORRO, L. P. & PORTÉ-AGEL, F. 2009 A wind-tunnel investigation of wind-turbine wakes: boundary-layer turbulence effects. *Boundary-Layer Meteorol.* **132** (1), 129–149.

COSSU, C., PUJALS, G. & DEPARDON, S. 2009 Optimal transient growth and very large-scale structures in turbulent boundary layers. *J. Fluid Mech.* **619**, 79–94.

CROUCH, J. D., GARBARUK, A. & MAGIDOV, D. 2007 Predicting the onset of flow unsteadiness based on global instability. *J. Comput. Phys.* **224**, 924–940.

ESPAÑA, M., AUBRUN, S., LOYER, S. & DEVINANT, P. 2011 Spatial study of the wake meandering using modelled wind turbines in a wind tunnel. *J. Wind Energy* **14** (7), 923–937.

IUNGO, G. V., VIOLA, F., CAMARRI, S., PORTÉ AGEL, F. & GALLAIRE, F. 2013 Linear stability analysis of wind turbine wakes performed on wind tunnel measurements. *J. Fluid Mech.* **737**, 499–526.

KANG, S., YANG, X. & SOTIROPOULOS, F. 2014 On the onset of wake meandering for an axial flow turbine in a turbulent open channel flow. *J. Fluid Mech.* **744**, 376–403.

KITSIOS, V., CORDIER, L., BONNET, J.-P., OOI, A. & SORIA, J. 2010 Development of a nonlinear eddy-viscosity closure for the triple-decomposition stability analysis of a turbulent channel. *J. Fluid Mech.* **664**, 74–107.

KITSIOS, V., CORDIER, L., BONNET, J.-P., OOI, A. & SORIA, J. 2011 On the coherent structures and stability properties of a leading-edge separated aerofoil with turbulent recirculation. *J. Fluid Mech.* **683**, 395–416.

MEDICI, D. & ALFREDSSON, P. H. 2006 Mesurements on a wind turbine wake: 3D effects and bluff body vortex shedding. *Wind Energy* **9** (3), 219–236.

MEDICI, D. & ALFREDSSON, P. H. 2008 Measurements behind model wind turbines: further evidence of wake meandering. *Wind Energy* **11**, 211–217.

MELIGA, P., PUJALS, G. & SERRE, E. 2012 Sensitivity of 2-D turbulent flow past a D-shaped cylinder using global stability. *Phys. Fluids* **24**, 061701.

OBERLEITHNER, K., PASCHEREIT, C. O. & WYGNANSKI, I. 2014 On the impact of swirl on the growth of coherent structures. *J. Fluid Mech.* **741**, 156–199.

OKULOV, V. L., NAUMOV, I. V., MIKKELSEN, R. F., KABARDIN, I. K. & SØRENSEN, J. 2014 A regular Strouhal number for large-scale instability in the far wake of a rotor. *J. Fluid Mech.* **747**, 369–380.

POPE, S. B. 2000 *Turbulent Flows*. Cambridge University Press.

REAU, N. & TUMIN, A. 2002 On harmonic perturbations in a turbulent mixing layer. *Eur. J. Mech. (B/Fluids)* **21** (2), 143–155.

REYNOLDS, W. C. & HUSSAIN, K. M. 1972 The mechanics of an organized wave in turbulent shear flow. Part 3. Theoretical models and comparisons with experiments. *J. Fluid Mech.* **54**, 263–288.

WU, Y. T. & PORTÉ-AGEL, F. 2011 Large-eddy simulation of wind-turbine wakes: evaluation of turbine parametrisations. *Boundary-Layer Meteorol.* **138** (3), 345–366.

ZHANG, W., MARKFORT, C. D. & PORTÉ-AGEL, F. 2012 Near-wake flow structure downwind of a wind turbine in a turbulent boundary layer. *Exp. Fluids* **52** (5), 1219–1235.